
RESEARCH ARTICLE

Journal Section

Fossil Image Identification using Deep Learning Ensembles of Data Augmented Multiviews

Chengbin Hou^{1,4*} | Xinyu Lin^{2,4*} | Hanhui Huang^{3*} |
Sheng Xu² | Junxuan Fan³ | Yukun Shi^{3†} | Hairong
Lv^{1,4†}

¹Department of Automation, Tsinghua University, Beijing, 100084, China

²College of Physics and Information Engineering, Fuzhou University, Fuzhou, 350108, China

³School of Earth Sciences and Engineering and Frontiers Science Center for Critical Earth Material Cycling, Nanjing University, Nanjing, China

⁴Fuzhou Institute of Data Technology, Fuzhou, 350200, China

Correspondence

Yukun Shi, Hairong Lv
Email: ykshi@nju.edu.cn;
lvhairong@tsinghua.edu.cn

Funding information

Natural Science Foundation of China, Grant Number: 42050101 and 42250104; National Key R&D Program of China, Grant Number: 2018YFE0204201 and 2021YFB3600401; Fujian Provincial Natural Science Foundation, Grant Number: 2021J01586

Abstract

1. Identification of fossil species is crucial to evolutionary studies. Recent advances from deep learning have shown promising prospects in fossil image identification. However, the quantity and quality of labeled fossil images are often limited due to fossil preservation, conditioned sampling, and expensive and inconsistent label annotation by domain experts, which pose great challenges to the training of deep learning based image classification models.

2. To address these challenges, we follow the idea of the wisdom of crowds and propose a novel multiview ensemble framework, which collects multiple views of each fossil specimen image reflecting its different characteristics to train multiple base deep learning models and then makes final decisions via soft voting. We further develop OGS method that integrates original, gray, and skeleton views under this framework to demonstrate the effectiveness.

3. Experimental results on the fusulinid fossil dataset over five deep learning based milestone models show that OGS using three base models consistently outperforms the baseline using a single base model, and the ablation study verifies the usefulness of each selected view. Besides, OGS obtains the superior or comparable performance compared to the method under well-known bagging framework. Moreover, as the available training data decreases, the proposed framework achieves more performance gains compared to the baseline. Furthermore, a consistency test with two human

* Equally contributing authors.

experts shows that OGS obtains the highest agreement with both the labels of dataset and the two experts.

4. We conclude that the proposed multiview ensemble framework and OGS method present the state-of-the-art performance in the fusulinid fossil identification case study. This methodology is designed for general fossil identification and it is expected to see applications on other fossil datasets. Notably, the result, which shows more performance gains as the train ratio decreases, suggests the potential application when the quantity of labeled data is particularly restricted, e.g., to identify rare fossil images. The consistency test indicates that the model can integrate the opinions of multiple experts, thus demonstrating its potential for dealing with inconsistencies in fossil identification.

KEYWORDS

fossil identification, deep learning, ensemble, multiview, fusulinid

1 | INTRODUCTION

Evolutionary studies require the accurate and efficient identification of extant and especially fossil species, however the hope is often frustrated by several restrictions. Most fossil species and many extant species are defined by their phenetic characters, and thus type specimens need to be assigned to represent their typical morphology. Due to the limited accessibility of type specimens, identification often relies on images, which presents challenges for researchers. This problem is particularly serious for paleontologists, as fossil species assignment is usually based on a small number of samples in varying states of preservation (Behrensmeyer *et al.*, 2000; Schopf, 1975; Foote and Raup, 1996; Holland, 2016), compared to extant species samples that are more abundant and readily available. Moreover, as research in the life and earth sciences tends to assemble more data for larger-scale, higher-resolution studies, the relatively small community of taxonomists faces greater challenges (MacLeod *et al.*, 2010, 2007). These issues highlight the increasing need for auxiliary tools or automatic identification systems to aid taxonomists in improving the efficiency and accuracy of their identification, and make large-scale studies with well-identified samples feasible.

Automatic identification models have remained heavily practiced in current biological and ecological studies for years, with numerous studies focusing on the identification of extant species (Wäldchen and Mäder, 2018; Borowiec *et al.*, 2022); however, there has been less focus on applying them to the studies of deep time. Fossil species are as rich in morphological diversity as modern organisms, but the available material is severely limited by fossil preservation and sampling intensity, which affects model training. With a limited number of samples, the model may not be able to fully learn the differences in features across categories, making it challenging to train effectively, or it may overfit, resulting in poor performance on the test set or in real-world applications. Another concern is the quality of fossil images, which is typically worse than that of modern species because the formation, burial, and sampling conditions of fossils can greatly alter the images, posing a greater challenge to the recognition ability of the model. The problem also lies in the labeling process. Taxonomic and systematic studies of some fossil groups, mostly relying on limited morphological information due to the general lack of molecular data, are insufficient and sometimes contradictory. This leads to disagreement among experts, causing inconsistency in data annotation and therefore affecting the training

of supervised learning models.

Nonetheless, recent advances in the use of deep learning models for taxonomic recognition have shown promising prospects for automated fossil species identification, including foraminifera (Hsiang *et al.*, 2019; Mitra *et al.*, 2019; Marchant *et al.*, 2020; Pires *et al.*, 2020), graptolites (Niu and Xu, 2022), fossil leaves (Wilf *et al.*, 2021), and multiple-body-fossil mixture (Liu *et al.*, 2022). The identification of modern foraminifera could be well compared to that of fossil foraminifera due to their close morphology and modes of preservation, and they are also among the first to be tested for species identification using deep learning. In their excellent study (Hsiang *et al.*, 2019), Hsiang *et al.* constructed a large image dataset of over 34,000 planktonic foraminifera and used most of these images to train three commonly used neural networks, VGG-16, DenseNet-121, and Inception-v3, for species-level identifications, achieving a maximum accuracy of 87.4%, which can compete with the expert accuracy of 63% to 85%. Another study (Mitra *et al.*, 2019), also conducted on modern foraminifera, performed a more systematic comparison of human expert versus machine performance. Their results revealed that the combination of VGG-16 and ResNet-50 neural networks could achieve an accuracy of at least 80%, while the performance of 11 human identifiers varied dramatically with an average accuracy of 63%. These studies show the promise of deep learning for fossil species identification. However, many thorny issues might arise as the categories and ages of fossils expand.

To delve into the automatic identification for fossils, we take fusulinids, a large group of fossil foraminifera dating back to c. 300 Ma, as the subject of our study. Fusulinids are the earliest larger benthic foraminifera that appeared in the shallow water of the Carboniferous and survived until the Late Permian (Pawłowski *et al.*, 2003; Vachard *et al.*, 2010). Their rapid evolution, as seen in morphological changes, makes them prominent index fossils for the Late Paleozoic biostratigraphy (i.e., dating the bearing rocks) (Ross and Ross, 1991; BouDagher-Fadel, 2008). Unlike modern foraminifera, fusulinids are primarily preserved in rocks that are difficult to separate, and studies are typically conducted on thin slices of the fossils that have been professionally made from rocks. This procedure compresses the three-dimensional morphological features into two dimensions, which is also common in the studies of other fossils such as corals, brachiopods, archaeocyathids, plants, and even vertebrate bones. To meet different research needs, multiple sections of fusulinid fossils, including axial, sagittal, and tangential sections, could be produced, and axial sections are preferred for identification as they contain the most useful features (Vachard *et al.*, 2010; Sheng *et al.*, 1988). This slice-based identification of fusulinids is very beneficial for the application of automatic identification models, as deep learning models based on two-dimensional images have already been well developed. The use of deep learning on fusulinid identification is a rather unexplored subject and, to our knowledge, only one study by Pires *et al.* (Pires *et al.*, 2020) serves as an example. They collected images of fusulinids from thin-slice micrographs and literature to construct a dataset containing 348 images of eight genera. Five standard neural network models (VGG-19, Inception-v3, MobileNet-v2, ResNet-50, and DenseNet-121) were trained on their dataset using transfer learning, and a maximum accuracy of 89% was achieved on Inception-v3 (Pires *et al.*, 2020). Although the dataset they used is small and has a rather uneven distribution of categories (the smallest category has only 15 images, while the largest has 88), it still provides extremely valuable feasibility validation.

In this work, we present the largest image dataset of fusulinids (Huang and Shi, 2022) to date, containing 2400 images from 16 genera that cover all six fusulinid subfamilies with respect to the classification system of Sheng *et al.* (Sheng *et al.*, 1988). Distinguished from the previous fossil identification studies that directly apply the existing machine learning and deep learning models, we follow the idea of "wisdom of crowds" and propose a novel framework (or meta method) to further improve the performance of existing deep learning models. Specifically, to compensate for the image quality and sample size, the fossil images in the original form are transformed into other forms (referred to as "views") so that some features are more pronounced for identification by deep learning models. These multiple views of training images with their labels are then fed respectively to train multiple base models. During inference,

the multiple views of test images are accordingly fed to corresponding base models to make individual predictions. These predictions are then combined to provide the final predictions. In machine learning, the proposed framework is related to the bagging framework (Zhou, 2021), both with respect to the concept of ensemble learning. The concept of ensemble learning is rarely used in fossil image classification, although recent research has shown the advantage of applying it to deep learning models (Dong *et al.*, 2020). The main novelty of the proposed framework lies in the input to each base model. The choice of input views depends on the characteristics of concrete applications, e.g., taking the skeleton view as the input could be worth trying for fusulinid fossil identification, as demonstrated in this work. Based on the proposed framework and the characteristics of fusulinids, we develop the OGS method that feeds the original view, gray view, and skeleton view of fusulinid images to three base models respectively. We select the deep learning milestone models, ResNet, MobileNet, Inception, EfficientNet, and RegNet, as the base model to validate the effectiveness of the proposed framework and the OGS method.

The main contributions of this work are summarized as follows. First, we propose a multiview ensemble framework rather than a specific method, which can be broadly applied to various deep learning image classification models and applied to fossil image identification or even more general image classification problem. Second, considering the characteristics of fossil images, we develop the OGS method based on the proposed framework and demonstrate the merits of OGS through extensive experiments. Third, the reasons why the proposed framework and OGS method achieve superior results are carefully discussed through further experiments, explanations, and calculations. Finally, the source code of proposed framework is publicly available¹ to benefit future research in fossil image identification.

2 | MATERIALS AND METHODS

2.1 | Dataset

The dataset used in this work is called "Fusulinid images 2400 - NJU", which is available at DDE repository (Huang and Shi, 2022). It consists of 2,400 thin-slice images of fusulinid individuals, including 291 microscope photos and 2,109 scanned images from the literature. The images are stored as PNG files with the transparency channel annotating the outline of the fossils and labeled according to their species name and data source. The 2,400 images are selected evenly from 16 genera of all six fusulinid families: Fusulinidae, Schwagerinidae, Ozawainellidae, Schubertellidae, Neoschwagerinidae, and Verbeekinae (see Table 1). Images of holotypes, paratypes, cotypes, and syntypes of the selected species are preferably chosen as they better represent the described morphological features. Although the images are labeled to the specific level, using this level would result in a significantly imbalanced data volume, so the generic level was chosen in our study.

2.2 | Problem Formulation

The fossil identification problem is a typical multiclass image classification problem. Considering a fossil dataset with totally k classes (species, genera, or other taxonomic ranks), the aim is to build a classification model f such that it can successfully predict a correct label for a given input image. In this work, a set of known labeled data $\{(\mathbf{X}_{img}, y), \dots\}$ are given for training. Each class $y \in \{1, 2, 3, \dots, k\}$ has at least one training sample. We build model f with trainable parameters, and train f using the training set. After that, the trained f can be used to predict label \hat{y} given an unlabeled image \mathbf{X}_{img} .

¹<https://github.com/houchengbin/Fossil-ID-Multiview-Deep-Ensembles>

TABLE 1 Overview of the taxonomy and number of images in the dataset. Generic level is used in this work. The classification system follows that of Sheng *et al.* (1988).

the Family	Subfamily	Genus	Number of images
Fusulinidae	Fusulininae	<i>Fusulina</i>	150
Fusulinidae	Fusulinellinae	<i>Fusulinella</i>	150
Fusulinidae	Staffellinae	<i>Nankinella</i>	150
Schwagerinidae	Schwagerininae	<i>Chusenella</i>	150
Schwagerinidae	Schwagerininae	<i>Eoparafusulina</i>	150
Schwagerinidae	Schwagerininae	<i>Parafusulina</i>	150
Schwagerinidae	Schwagerininae	<i>Pseudofusulina</i>	150
Schwagerinidae	Schwagerininae	<i>Quasifusulina</i>	150
Schwagerinidae	Schwagerininae	<i>Rugosofusulina</i>	150
Schwagerinidae	Schwagerininae	<i>Schwagerina</i>	150
Schwagerinidae	Schwagerininae	<i>Triticites</i>	150
Schwagerinidae	Pseudoschwagerininae	<i>Pseudoschwagerina</i>	150
Ozawainellidae	Ozawainellinae	<i>Eostaffella</i>	150
Schubertellidae	Schubertellinae	<i>Schubertella</i>	150
Neoschwagerinidae	Neoschwagerininae	<i>Neoschwagerina</i>	150
Verbeekinidae	Misellininae	<i>Misellina</i>	150

2.3 | Method

2.3.1 | Overview

This work introduces a framework or a meta method (rather than a specific method) for fossil identification problem. The purpose is to further improve the performance of representative deep learning models for fossil classification. Figure 1 elaborates the overview of the proposed framework. Concretely, we employ multiple base models to learn from the multiviews of the original input fossil images. Each base model and view are one-to-one correspondence, so that each base model can extract diverse features for making individual predictions. There could be many different choices of the multiviews of original images, such as simple duplication or meaningful transformations. The final decision is made by combining the predictions from multiple classifiers following the "wisdom of crowds" idea.

2.3.2 | Base Models

The base models are the fundamental components of the proposed framework. The qualified base models should first be the candidate for solving the problem formulated in Section 2.2. Since the problem to solve is a typical multiclass image classification problem, a large number of models based on deep convolutional neural networks can be adopted as the base models for this problem (Li *et al.*, 2021). Essentially, the base model tries to automatically extract proper image features using the convolutional filters, such that these features are discriminative for making correct predictions. Each base model is trained using one view of the labeled images, and the error (via cross-entropy) between the predicted label (a predicted probability distribution over all classes) and the ground truth label (a probability distribution where 1 for the class of the label and 0 for other classes) is back propagated to adjust the trainable parameters in deep learning models. After training, we obtain the trained base model f_{base} which can map or transform an (either

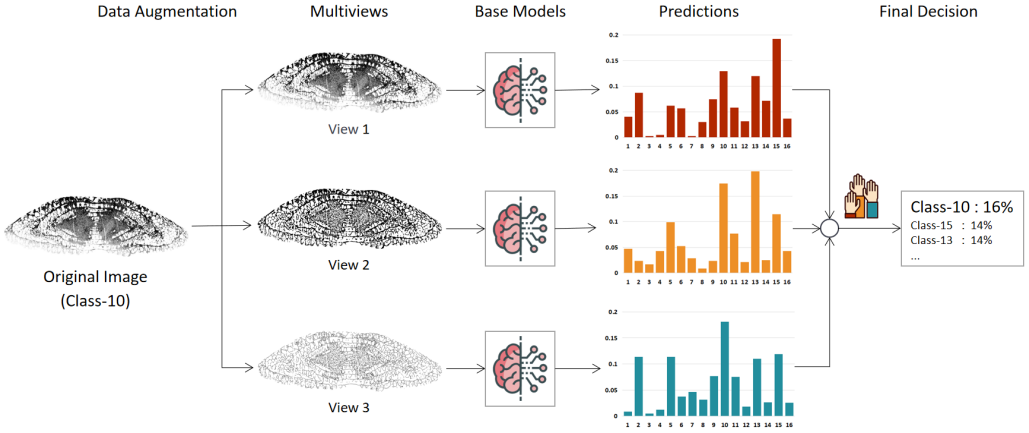


FIGURE 1 Overview of the proposed framework. Multiple base models, taking three as an example, are dedicated to individually learn from the multiviews of original input images. The multiviews are desirable to come from the meaningful data augmentation techniques (e.g., skeletonization) related to the specific image domain (e.g., fossil domain). The final decision is made by combining the predictions from multiple base models.

seen or unseen) input image X_{image} to a probability distribution \mathbf{z} overall k classes, i.e.,

$$f_{base} : X_{image} \mapsto \mathbf{z} \in \mathbb{R}^k \quad (1)$$

The selected milestones of deep learning models for image classification are summarized below. These models, with the latest data argumentation and the state-of-the-art updates by famous deep learning library TIMM² and also with the pretrained model parameters from ImageNet dataset, are respectively employed as the base model f_{base} of the proposed multiview ensemble framework.

- ResNet or Residual Network (He *et al.*, 2016) is one of the representative types of convolutional neural networks (CNN), which aims to effectively include more convolutional layers in CNN using skip connections between some layers. The specific ResNet adopted in this work is ResNet-50³ that additionally uses a bottleneck design to improve the efficiency of the training process.
- MobileNet (Howard *et al.*, 2017) is a light model that greatly reduces the number of parameters in CNN, and is originally designed for mobile devices. MobileNet-v3 (more specifically MobileNet-v3-large-100)⁴ is tested in this work. It utilizes the neural architecture search technique (Zoph and Le, 2016) to modify MobileNet so as to improve both effectiveness and efficiency.
- Inception-v4 (Szegedy *et al.*, 2017) is a CNN model developed from Inception-v1 also known as GoogLeNet (Szegedy *et al.*, 2015) where the inception module is introduced. Batch normalization and factorization are then introduced in Inception-v2 and Inception-v3 respectively. Comparing to Inception-v3, Inception-v4⁵ has the simplified architecture (without residual connections) with more inception modules, and shows the higher accuracy in ImageNet classification task.

²<https://timm.fast.ai>

³<https://rwightman.github.io/pytorch-image-models/models/resnet>

⁴<https://rwightman.github.io/pytorch-image-models/models/mobilenet-v3>

⁵<https://rwightman.github.io/pytorch-image-models/models/inception-v4>

- EfficientNet (Tan and Le, 2019) presents a novel approach to uniformly scale width, depth, and resolution over a base CNN model using a compound coefficient (given that coefficient in a constraint optimization for width, depth, and resolution). EfficientNet-b0 is based on a variant of MobileNet-v2 (Tan and Le, 2019). There are eight versions from b0 to b7 corresponding to increasing compound coefficients and model parameters. Considering the relative small dataset in experiments, EfficientNet-b2⁶ is chosen for the experiments.
- RegNet (Radosavovic *et al.*, 2020) is a simple network design space coming from the neural architecture search (Zoph and Le, 2016) over a large network design space. The network design space of RegNet is restricted by the quantized linear function for widths and depths. RegNetX has another two restrictions, while RegNetY further includes squeeze-and-excitation blocks. RegNetY (more specifically RegNetY-032)⁷ is experimented in this work.

2.3.3 | Data Augmented Multiviews

The purpose of multiviews is to encourage base models to make good individual predictions. More specifically, each base model should gain good performance and meanwhile be complementary to each other, i.e., base models are good at classifying different sets of classes. The classical bagging strategy (Zhou, 2021) that creates multiple random subsets of the original training set would likely reduce the available unique training data at each view. To alleviate this challenge, the most regular method is to duplicate the original training set for each view, which gives the naive version called OOO when considering three views. In order to increase the diversity between the three views and base models, we further propose two extra meaningful views called gray view (ignoring RGB color) and skeleton view (focusing on outline), and accordingly come up with the augmented version called OGS. There could be other possible meaningful transformations, other combinations of views, and even much more views. We provide preliminary research in this direction and leave others as future work. Formally, we have

$$f_{trans_1}, f_{trans_2}, \dots, f_{trans_m} : \mathbf{X}_{image} \mapsto \mathbf{X}_{view_1}, \mathbf{X}_{view_2}, \dots, \mathbf{X}_{view_m} \quad (2)$$

where the function f_{trans_m} transforms the original image \mathbf{X}_{image} to view m and produces augmented image \mathbf{X}_{view_m} . Letting $m = 3$, for naive version OOO, $f_{trans_1}, f_{trans_2}, f_{trans_3} = I, I, I$ where I is identity matrix. Regarding OGS, f_{trans_2} converts original images to gray images via $Gray = 0.299R + 0.587G + 0.114B$ where R is for the red channel, G is for the green channel, and B is for the blue channel of the original images. f_{trans_3} converts the gray images to binary images, and then employs Zhang's method (Zhang and Suen, 1984) for skeletonization that reduces binary objects to one pixel-wide representation.

2.3.4 | Ensemble Mechanism

To reduce the risk of overfitting due to the limited and expensive labeled fossil data, we maintain the number of unique training data at each view by data augmentation as described in Section 2.3.3, which is distinguished from bagging strategy (Dong *et al.*, 2020). The m views of original images \mathbf{X}_{view_m} are respectively fed to m base models f_{base_m} , and produce m probability distribution \mathbf{z}_m over k classes. For each view and base model, we mathematically have

$$\mathbf{z}_m = f_{base_m}(\mathbf{X}_{view_m}), \quad \mathbf{z}_m \in \mathbb{R}^k \quad (3)$$

⁶<https://rwightman.github.io/pytorch-image-models/models/efficientnet>

⁷<https://rwightman.github.io/pytorch-image-models/models/regnety>

Each base model is trained using the same number of training data $\{(X_{view_m}, y), \dots\}$ from each view. The trainable parameters in f_{base_m} are optimized by gradually reducing the error between the predicted class probability distribution z_m and ground truth label probability distribution (i.e., one-hot vector). After training, each base model f_{base_m} can be used to make its own predictions z_m given the corresponding augmented image X_{view_m} . Following the idea of "wisdom of crowds", the final decision are made via

$$\hat{y} = \arg \max_k z = \arg \max_k f_{comb}(z_1, z_2, \dots, z_m) \quad (4)$$

where function f_{comb} combines the predictions z_1, z_2, \dots, z_m from m views and models, and produces the final prediction or final probability distribution z . Note that, m is set to three in this work, and we take soft voting, i.e., $f_{comb}(z_1, z_2, z_3) = (z_1 + z_2 + z_3)/3$ for combining the predictions. The operator $\arg \max$ over k means finding the maximum probability in vector $z \in \mathbb{R}^k$ and return the corresponding index as the predicted label \hat{y} .

2.4 | Experimental Settings

The fusulinid dataset consists of 2,400 images of fusulinid individuals from 16 genera, and therefore 16 classes in our case, with 150 images each. Regarding the multiclass classification problem, the widely-used Acc@1 (true class matching with the top-1 probable predicted class, which is equivalent to Micro-F1 in our case), Acc@3 (true class matching with the top-3 probable predicted classes), and Macro-F1 (harmonic mean of precision and recall over classes) are adopted as the metrics to evaluate the performance of the trained model in predicting test images.

For hyper-parameters, we search learning rate [0.001, 0.01, 0.1] and batch size [32, 64, 128] for each base model (totally nine combinations), and set the epoch to 500 and use the default TIMM hyper-parameters for others. The best hyper-parameters of each model for original, gray, and skeleton views, are selected respectively by comparing the average of two independent runs of Acc@1 results. And these hyper-parameters are then employed in the following experiments. The experiments are conducted on the GPU server, NVIDIA GeForce RTX 3090 Ti with 24G memory. For reproducibility, Table 2 lists the best hyper-parameters that are adopted in following experiments.

TABLE 2 The best parameters (learning rate, batch size) of each model for original, gray, and skeleton views.

	ResNet-50	MobileNet-v3	Inception-v4	EfficientNet-b2	RegNetY
Original View	(0.01, 32)	(0.1, 64)	(0.1, 32)	(0.01, 32)	(0.1, 128)
Gray View	(0.1, 64)	(0.1, 128)	(0.1, 64)	(0.1, 128)	(0.01, 32)
Skeleton View	(0.1, 32)	(0.01, 32)	(0.1, 64)	(0.1, 32)	(0.1, 128)

3 | RESULTS

3.1 | Main Experiments

In the main experiments, we feed the majority of data with labels to train the model. Specifically, each class has 110 images for training and 20 images each for validation and testing. Table 3 presents comprehensive comparisons that not only the OOO and OGS methods as described in Section 2.3, but also several combinations of one and two view ensembles based on the proposed multiview framework.

TABLE 3 The results of combinations of one, two, and three views’ methods under the proposed ensembles of data augmented multiviews framework. The abbreviation O, G, and S are for original, gray, and skeleton views respectively. The results along the O column are the baseline that directly trains the base model using original images. The top-2 performances along each row are in bold, and the top-1 is also marked with †. Each entry describes the mean \pm standard deviation obtained from 20 independent runs.

Acc@1									
	O	OO	OOO	OGS	OG	OS	GS	G	S
ResNet-50	87.98 \pm 1.19	88.84 \pm 0.85	88.88 \pm 0.80	90.30 [†] \pm 0.65	89.27 \pm 0.68	89.44 \pm 1.09	89.42 \pm 1.03	88.78 \pm 0.86	83.78 \pm 1.51
MobileNet-v3	90.23 \pm 1.19	91.14 \pm 0.65	91.33 \pm 0.65	91.59 [†] \pm 0.66	91.28 \pm 0.78	91.00 \pm 0.86	91.11 \pm 0.49	90.72 \pm 0.75	85.33 \pm 1.01
Inception-v4	89.78 \pm 1.13	90.77 \pm 0.72	91.16 [†] \pm 0.70	91.16 [†] \pm 0.79	91.11 \pm 1.04	89.91 \pm 0.93	90.05 \pm 0.82	89.63 \pm 1.18	85.39 \pm 1.52
EfficientNet-b2	90.72 \pm 0.50	90.61 \pm 0.39	90.48 \pm 0.49	91.53 [†] \pm 0.77	91.11 \pm 0.63	90.19 \pm 1.08	90.61 \pm 1.12	90.33 \pm 0.79	85.92 \pm 1.47
RegNetY	90.30 \pm 0.81	91.27 \pm 0.81	91.59 [†] \pm 0.75	91.41 \pm 0.81	91.33 \pm 0.82	90.25 \pm 1.06	89.84 \pm 0.54	90.03 \pm 0.92	85.23 \pm 1.51
Acc@3									
	O	OO	OOO	OGS	OG	OS	GS	G	S
ResNet-50	97.64 \pm 0.47	97.92 \pm 0.43	98.08 \pm 0.42	98.47 [†] \pm 0.42	98.13 \pm 0.38	98.06 \pm 0.56	98.02 \pm 0.59	97.42 \pm 0.70	95.55 \pm 0.73
MobileNet-v3	98.00 \pm 0.58	98.42 \pm 0.55	98.56 \pm 0.30	98.64 [†] \pm 0.36	98.58 \pm 0.42	98.14 \pm 0.44	98.20 \pm 0.44	98.02 \pm 0.49	96.13 \pm 0.71
Inception-v4	98.06 \pm 0.58	98.53 \pm 0.42	98.64 [†] \pm 0.43	98.47 \pm 0.48	98.52 \pm 0.49	98.22 \pm 0.41	98.25 \pm 0.54	97.98 \pm 0.64	96.47 \pm 0.63
EfficientNet-b2	97.70 \pm 0.57	97.97 \pm 0.63	98.06 \pm 0.54	98.42 [†] \pm 0.44	98.23 \pm 0.43	98.11 \pm 0.39	98.05 \pm 0.45	97.84 \pm 0.71	95.72 \pm 0.90
RegNetY	97.03 \pm 0.64	97.72 \pm 0.59	97.91 \pm 0.46	98.31 [†] \pm 0.61	97.52 \pm 0.78	97.91 \pm 0.63	98.17 \pm 0.59	97.16 \pm 0.75	96.59 \pm 0.81
Macro-F1									
	O	OO	OOO	OGS	OG	OS	GS	G	S
ResNet-50	87.73 \pm 1.18	88.61 \pm 0.85	88.69 \pm 0.81	90.23 [†] \pm 0.67	89.07 \pm 0.72	89.39 \pm 1.10	89.41 \pm 1.05	88.67 \pm 0.87	83.67 \pm 1.58
MobileNet-v3	90.14 \pm 1.19	91.09 \pm 0.65	91.25 \pm 0.67	91.55 [†] \pm 0.69	91.21 \pm 0.79	90.94 \pm 0.85	91.09 \pm 0.49	90.67 \pm 0.78	85.24 \pm 1.03
Inception-v4	89.62 \pm 1.24	90.61 \pm 0.79	91.03 \pm 0.73	91.09 [†] \pm 0.81	90.98 \pm 1.09	89.82 \pm 0.97	89.96 \pm 0.85	89.51 \pm 1.19	85.38 \pm 1.55
EfficientNet-b2	90.55 \pm 0.51	90.43 \pm 0.40	90.31 \pm 0.50	91.44 [†] \pm 0.79	90.99 \pm 0.65	90.10 \pm 1.08	90.57 \pm 1.13	90.25 \pm 0.79	85.92 \pm 1.47
RegNetY	90.20 \pm 0.83	91.17 \pm 0.82	91.48 [†] \pm 0.77	91.34 \pm 0.79	91.24 \pm 0.85	90.22 \pm 1.03	89.82 \pm 0.56	89.93 \pm 0.94	85.28 \pm 1.47

Some key observations from Table 3 are as follows. First, O, OO, and OOO show the naive ensembles of deep learning models can improve the performance in most cases but is saturated comparing to the (O, OO) and (OO, OOO) pairs; while EfficientNet-b2 might not enjoy improvement gained by such a naive ensemble. Second, OOO and OGS as well as O, G, and S demonstrate the ensembles of data augmented multiviews with gray and skeleton views, i.e., OGS, can further improve the performance in the same case of using ensembles of three views, though the simple average of the performance of O-O-O is higher than O-G-S. Third, Comparing to the O column, i.e., the baseline that simply trains the base model using original images, the ensemble of data augmented multiviews OGS consistently outperforms the baseline O with the gains ranging [0.81, 2.32], [0.41, 1.28], and [0.89, 2.5] for Acc@1, Acc@3, and Macro-F1 respectively. The improvement gains of Acc@3 are less than Acc@1, since Acc@1 is a stricter metric than Acc@3 as introduced in experimental settings. Fourth, OGS, OG, OS, and GS display an ablation study to prove the usefulness of each view exploited in this work, as lacking any view leads to performance degradation. Overall, OGS generally achieves the best performance regarding all the five typical deep learning image classification models and three widely-used multiclass classification evaluation metrics.

To compare the proposed framework and the classical bagging framework, we follow the standard bagging framework (Zhou, 2021) to implement OOO-bagging method. Concretely, the test set of OOO-bagging exactly follows that of OGS, i.e., first randomly taking out 20 test images for each class as described in the main experiments. For OOO-bagging, the same number of the remaining images are randomly sampled with replacement from the remaining images to create the training set (hence some images might be sampled multiple times), and the final rest of the images that are not sampled act as the validation set. The OOO-bagging method repeats such bootstrapping strategy three times from the original view and accordingly trains three base models to form ensembles. The performance comparison of the OOO-bagging method and the OGS method is illustrated in Figure 2.

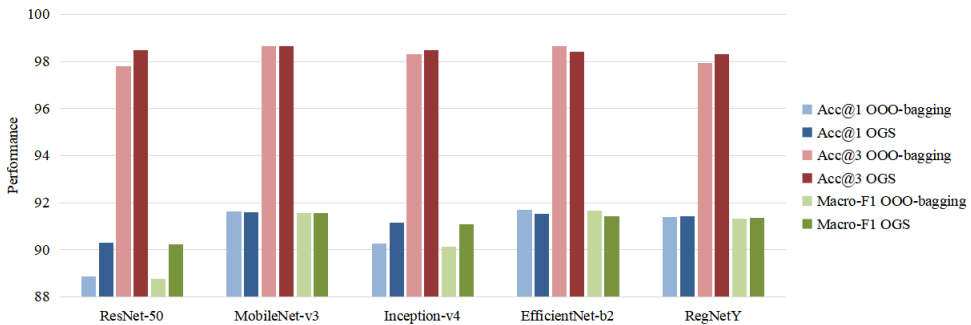


FIGURE 2 Bagging framework vs. the proposed framework. The method OGS under the proposed framework significantly outperforms the method OOO-bagging under the classical bagging framework for ResNet-50 and Inception-v4, though they obtain comparable performance for other base models. Best viewed in colors.

We observe that OGS significantly outperforms OOO-bagging for ResNet-50 and Inception-v4, though they obtain comparable performance for other base models. The results indicate that the proposed framework might be more effective than the classical bagging framework given the similar computational budget of the ensemble of three base models. The potential reason could be that the number of unique training data for OGS is more than that for OOO-bagging, which might therefore alleviate the overfitting issue due to insufficient training data.

3.2 | Different Ratio of Train Set

Machine learning models often need sufficient labeled data to train the model so as to relieve the potential overfitting issue. Nevertheless, it might be expensive or hard to annotate data, which is the typical case when it requires domain experts to do the annotation, like our case of fusulinids. To this end, we simulate such scenarios by decreasing training data. Specifically, the ratios of images in each class for train, validation, and test set are 0.1-0.8 (with step 0.1), 0.1, and 0.8-0.1 (with step 0.1) respectively, i.e., eight different data splits for benchmarks. We choose ResNet-50 (OGS achieving best results in Table 3), Inception-v4 (OGS and OOO obtaining similar results in Table 3) and RegNetY (OOO achieving best results in Table 3) for the experiments, and the results under different limited training data are illustrated in Figure 3.

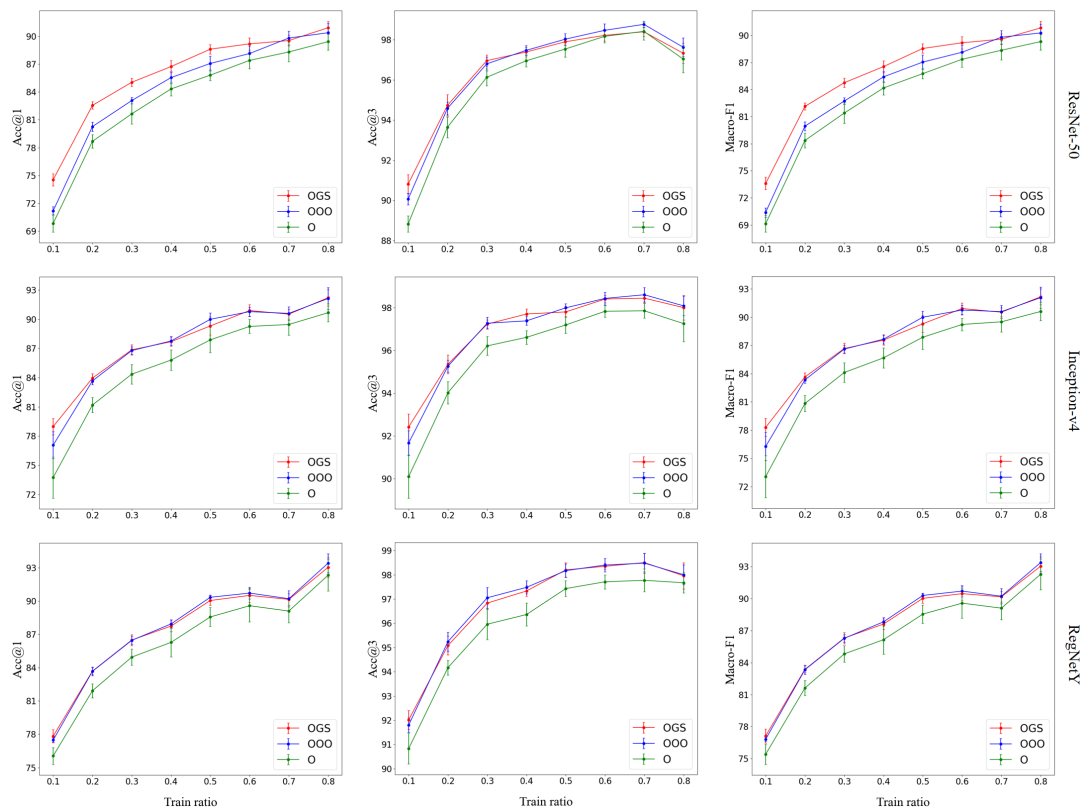


FIGURE 3 The results of Acc@1, Acc@3, and Macro-F1 (from left to right) under various train ratios (0.1-0.8 with step 0.1) for the base model ResNet-50 (row 1), Inception-v4 (row 2), and RegNetY (row 3). Best viewed in colors.

It is interesting to observe that as the train ratio decreases, OGS and OOO (under the proposed framework) obtain more performance gains compared with O which simply employs the original images to train a single base model of ResNet-50, Inception-v4, or RegNetY. Besides, the error bars of standard deviation of 10 independent runs indicate that OGS and OOO are more robust than O. Furthermore, OGS and OOO reach comparable performance for various training ratios when taking RegNetY as the base model; OGS obtains much better performance than OOO and O (e.g., 1.91% and 5.24% Acc@1 gains respectively) when considering the smallest train ratio 0.1 for Inception-v4 as the base

model, despite OGS and OOO obtain similar results when feeding about 0.733 of the dataset for training as shown in Table 3; OGS considerably outperforms OOO for most training ratios when taking ResNet-50 as the base model.

4 | DISCUSSION

4.1 | The superiority of the proposed framework and selected views

According to Table 3, OGS generally achieves the best performance for all the five types of base models and three widely-used metrics. Comparing to previous related studies, the optimal top-1 accuracy of OGS at 91.59% surpassed that of Pires *et al.* (2020) with the top-1 accuracy at 89%. As a balanced dataset with 16 genera is used in this work while their dataset contains a varying number of images for each of the 8 genera, our study presents the more representative framework for fusulinid with greater potential in real-world application. Also, this performance is superior to those practised on modern foraminifera with the accuracy of around 90% (Hsiang *et al.*, 2019; Mitra *et al.*, 2019; Marchant *et al.*, 2020). For the variants of OGS, i.e., OG, OS, and GS, Table 3 demonstrates that each view exploited is helpful, since the absence of any view results in performance degradation. In fact, there could be other possible views that researchers or engineers can further explore based on the characteristics of their own fossil images. Although the dataset adopted in this work is fusulinid image, it is worth mentioning that the proposed framework or meta method can be directly used or easily modified for broader fossil or extant organisms image classification problems.

Table 3 also suggests the superior performance of OGS against OOO, i.e., the data augmented three views would gain more benefits compared to the duplicated three views. The reason could owe to the improvement of the diversity of the predictions among three base models when the data augmented three views are fed to the three base models. To support this claim, we plot the confusion matrices of the original view, gray view, skeleton view, and multiview ensemble for ResNet-50 and EfficientNet-b2 as shown in Figure 4. We observe that the corresponding correct predictions (i.e., the numbers along the diagonal) of the multiview ensemble are greater than or equal to any one of the three views, mostly greater than or equal to two views of the three views, and partially greater than all three views, which implies that the three views can draw support from each other to further improve the performance. Apart from this general observation, the correct predictions of *Triticites* for O, G, and S views are 17, 16, and 13 respectively when the base model is ResNet-50, which boosts the performance to 19 correct predictions by the proposed framework of data augmented multiview ensemble. Similar observations can be found for *Schwagerina* on ResNet-50, *Eastaffella* on EfficientNet-b2, and so on. On the other hand, considering the incorrect predictions (i.e., the numbers not in diagonal), it shows that the same base model trained with different views yields diverse predictions. For example, the images of *Pseudoschwagerina* using ResNet-50 are misclassified to *Misellina* and *Triticites* when feeding original or gray images, whereas that are misclassified to *Fusulina* and *Schwagerina* when feeding skeleton images; such diverse predictions resulting from data augmented multiviews and utilizing the proposed ensemble framework finally revise the misclassifications of *Misellina*, *Fusulina*, and *Schwagerina* to the correct class of *Pseudoschwagerina*. Overall, the diversity that enhanced predictions of both correct and incorrect predictions could be why the data augmented three views can further improve the performance.

The mechanism by which the O, G, and S views help the ensemble model obtain the correct identification result is worth exploring. Fossils are preserved in sedimentary rocks, and the chemical composition of fossils can be greatly affected by the surrounding rocks and fluids during taphonomic processes (Behrensmeyer *et al.*, 2000; Martin, 1999), and differences in the composition can produce different colors that do not contain information regarding the fossil structure itself. Although the color may somewhat reflect differences in the living and preservation environments of various classes of fossils, the optical microscope used, the filming equipment and parameters, and the factors of

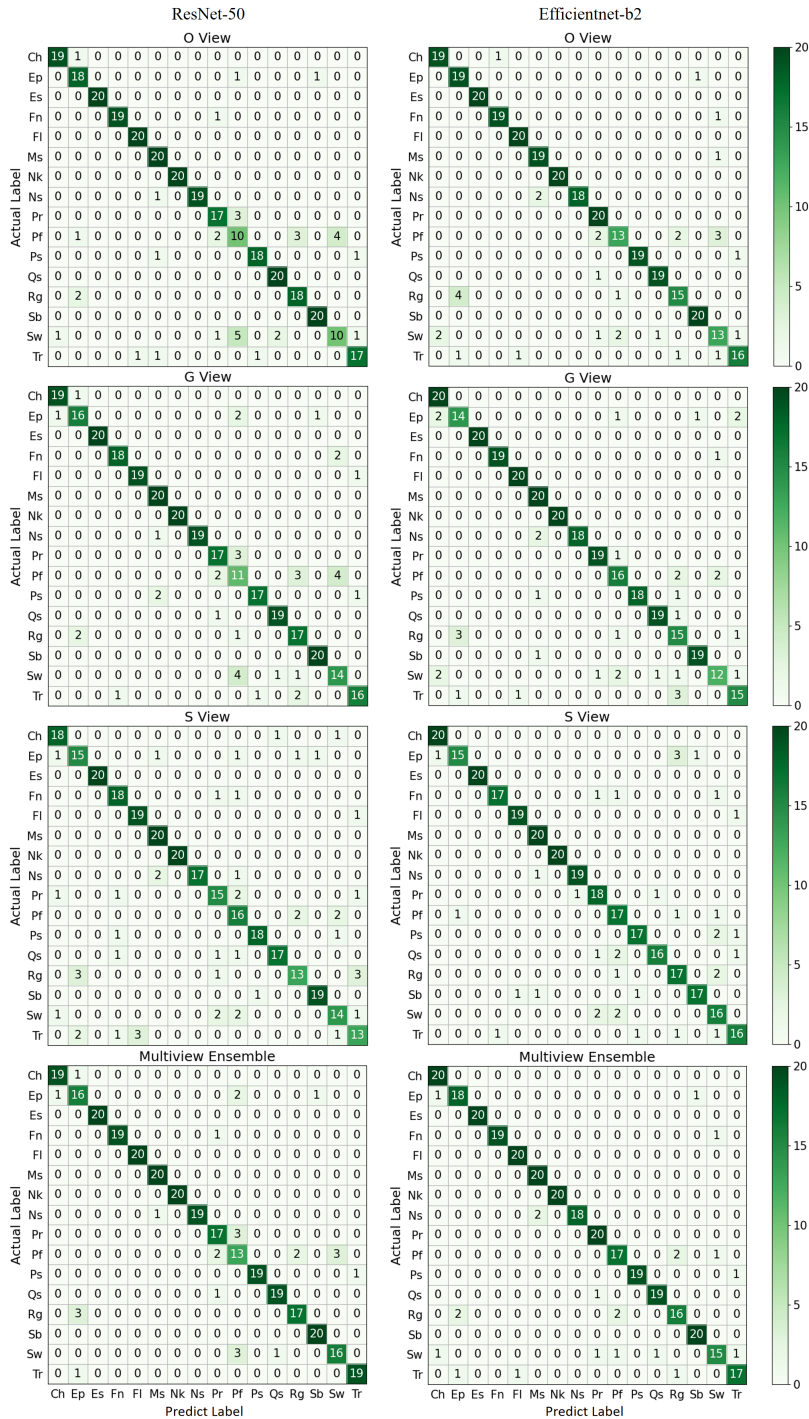


FIGURE 4 The confusion matrix for original view, gray view, skeleton view, and multiview ensemble (top-down) when the base model is ResNet-50 (left) or EfficientNet-b2 (right). The deeper color indicates the larger number, and the maximum number is 20. The number along the diagonal line represents the number of corrected predictions, i.e., the predicted label (x-axis) matches the actual label (y-axis). Best viewed in colors. **Abbr.** Ch, *Chusenella*; Ep, *Eoparafusulina*; Es, *Eostaffella*; Fn, *Fusulina*; Fl, *Fusulinella*; Ms, *Misellina*; Nk, *Nankinella*; Ns, *Neoschwagerina*; Pr, *Parafusulina*; Pf, *Pseudofusulina*; Ps, *Pseudoschwagerina*; Qs, *Quasifusulina*; Rg, *Rugosofusulina*; Sb, *Schubertella*; Sw, *Schwagerina*; Tr, *Triticites*.

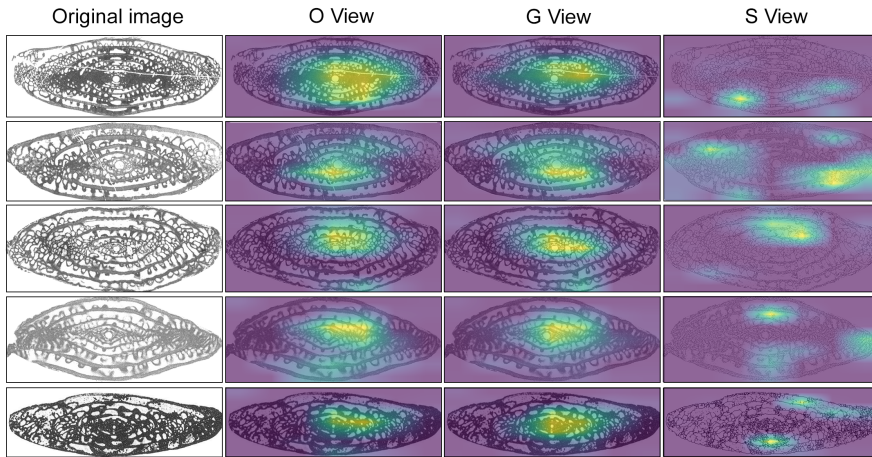


FIGURE 5 Examples of original images and corresponding visualization results of activation mapping of original view, gray view, and skeleton view (left-right), generated by Grad-CAM (Selvaraju *et al.*, 2016). The base model is ResNet-50, which is consistent with the model used in Figure 4. The five input images are from the species of subfamily Schwagerininae including *Parafusulina australis*, *Rugosofusulina mansuyi*, *Pseudofusulina wulungensis*, *Schwagerina neoaculata* and *Triticites kawensis* (top-down). These images are not to scale. The contribution of different regions to identification is indicated by a color ranging from purple to yellow. The yellow highlighted regions contribute the most. Note that the activated regions of the S view are clearly distinct from that of the other two, indicating different features detected and analyzed. Best viewed in colors.

printing and scanning may also introduce color-related noise. In our case, there is little difference in whether color information is included or not, as the performance of O and G does not show much comparable variance (see Table 3 and Figure 4). However, for other potential fossil groups, the removal of color may result in greater differences and requires caution. Conversion to skeletonized images is also useful as it helps represent the objects' topology and thus serves as a feature extraction (Saha *et al.*, 2016). For shell-forming organisms like fusulinids, the topology of their shell, such as the number and size of chambers and the manner of spinning and coiling, is sufficient to provide a great deal of information for their identification and classification (Vachard *et al.*, 2010; Sheng *et al.*, 1988; Ross and Ross, 1991). Skeletonization can be seen as a feature extractor based on this prior knowledge to help the model learn the topological features of the fossil.

The diversity in view may have led to their diversity in the extraction of fossil structural information. This is especially clear when it comes to the subfamily Schwagerininae (see the taxonomy in Table 1) and can be confirmed by Class Activation Mapping (CAM), a method that weighs the sum of the presence of visual patterns at different spatial locations and underlines the image regions most relevant to a particular category (Zhou *et al.*, 2015). Figure 5 shows the visualization of Grad-CAM (Selvaraju *et al.*, 2016) of O, G, and S on images of 5 individuals from the subfamily Schwagerininae, using timm-vis⁸. The first two views, O and G, tend to activate in the middle of the image, which is the region of the proloculus (very first coiling whorl of fusulinids) and the 2-3 inner whorls. The S view, on the other hand, is often dispersed and activates at the periphery of the fusulinid, which is the whorls grown at the later stage. Figure 4 shows that the S view particularly achieves better performance on the two schwagerine groups *Pseudofusulina* and *Schwagerina*, compared to the other two views (see the 10th and 15th diagonal elements of confusion matrices).

⁸<https://github.com/novice03/timm-vis>

These two fusulinid genera are morphologically very similar but distinguishable for the ontogenetic development process. The proloculus of *Pseudofusulina* is oftentimes large and the succeeding whorls coil very loosely, while the proloculus of *Schwagerina* is often small with the 2-3 succeeding whorls coiling intensely and gradually loosening outwards. Although the differences are distinct with regard to their development and fusulinid taxonomists agree to put them into two genera (Sheng *et al.*, 1988; Moore, 1964), controversies exist in the identification on a case-by-case basis (see part 4.3 for a consistency estimation). The skeleton view, as seen in the CAM result, may be able to highlight the differences in proloculus and outer whorls and therefore shows more excellence in these subtly distinguishable groups. In the case of ensemble learning, multiple views can complement each other by highlighting different features. Although the Grad-CAM results may not fully reflect the model's "attention" distribution, they are a good demonstration of the fact that a simple manipulation of fossil images (such as the skeletonization) can emphasize unique features of the identical individual for the model, so that the ensemble model can synthesize the classification information obtained from more aspects and reach the optimal results.

4.2 | Beneficial to small image datasets

The current multiview ensemble learning is especially suitable for small image datasets such as fossils. In Figure 3, the most significant finding is that as the training ratio of labeled images decreases, the proposed framework especially the OGS method often performs relatively better when compared to simply using one single model of the existing deep learning image classification model. This finding indicates that the proposed framework has a substantial application when the labeled data are insufficient. Fossil image data exactly fits into this category. While the fossil images are oftentimes limited as a result of fossil preservation and sampling intensity and the annotation of fossil images requires specific domain knowledge, and more frequently, detailed studies. Consequently, lacking labeled training data is a common challenge in the practice of fossil image identification and classification, and is hindering the advance of automatic identification methods. The proposed multiview ensemble framework is proven to be likely to perform much better than simply applying a single model provided insufficient training data, thus showing the promise for similar practices on other fossils, especially rare ones.

Figure 2 compares the proposed multiview ensemble framework with the most representative and similar ensemble framework, and the OGS method and OOO-bagging method are implemented respectively for comparison. OGS can significantly outperform OOO-bagging for ResNet-50 and Inception-v4. One possible reason could be that the number of unique training data for OGS is greater than that for OOO-bagging, which helps OGS alleviate the potential overfitting issue due to insufficient training data. For our case, based on the descriptions in Section 2.4 and Section 3.1, the number of unique training samples for each base model of OGS is 110 per class (or 1760 for all classes), while that of OOO-bagging is less than 110. Concretely, the bootstrapping strategy of OOO-bagging randomly takes the number of n samples with replacement from the given n samples. The number of unique training samples can be calculated via $1 + \frac{n-1}{n} + (\frac{n-1}{n})^2 + \dots + (\frac{n-1}{n})^{n-1}$ where the first term 1 is the probability of the first sample being non-repetitive; the second term $\frac{n-1}{n}$ is the probability of the second sample being non-repetitive; the third term $(\frac{n-1}{n})^2$ is the probability of the third sample being non-repetitive; and the last term is the probability of the n -th sample being non-repetitive. Applying the formula of summation for the geometric sequence, we finally derive $[1 - (\frac{n-1}{n})^n] \times n = [1 - (\frac{130-1}{130})^{130}] \times 130 \approx 0.6335 \times 130 = 82.355$ where $n = 130$ since there are 20 images per class reserved as test set, the number of unique training samples is around 82 images per class (or around 1318 images for all classes), and the remaining 48 images per class are used as the validation set. Therefore, the number of unique training samples to each base model for OOO-bagging is around 1318 regarding all classes, which is smaller than OGS with 1760 unique training samples, i.e., reducing $(1760 - 1318)/1760 \approx 25.11\%$ non-repetitive training samples.

4.3 | Identification consistency estimation

Another point to note is the label inconsistency, which may also be responsible for the misidentification of the model. The study uses supervised classification, i.e., each image needs to be pre-labeled, so whether the labels can consistently indicate the features of the object used for classification will greatly affect the final performance of the model. As mentioned earlier, the identification or classification of fossil species requires corresponding domain knowledge, and different experts use different morphological criteria due to different experience, training, and access to samples (MacLeod *et al.*, 2010, 2007; Fenton *et al.*, 2018), which leads to inconsistency in the labels they give. This inconsistency can be partially resolved by recalibration by an individual expert, but even when experts are the same person or work in the same laboratory, their self-consistency (consistency in results obtained from multiple practices of identification on the same sample) is not necessarily high (Fenton *et al.*, 2018; Culverhouse *et al.*, 2014). In the present study, the dataset used contains images from multiple sources, which may introduce label inconsistency despite the fact that the dataset has been subjected to some quality control (e.g., preferential use of holo- and paratype specimens). A consistency test is performed to explore the nature of such consistency within the dataset.

TABLE 4 The consistency rates between true labels and identification results obtained by the OGS model and two human experts. The consistency test is performed on a test set of 8 genera of the family Schwagerinidae (*Eoparafusulina*, *Parafusulina*, *Pseudofusulina*, *Pseudoschwagerina*, *Quasifusulina*, *Rugosofusulina*, *Schwagerina*, and *Triticites*), with 20 images each. The OGS ensemble model is aligned with that of Figure 4 and 5.

	Label	OGS	Expert 1	Expert 2
Label	1	0.85	0.68	0.57
OGS		1	0.68	0.58
Expert 1			1	0.53
Expert 2				1

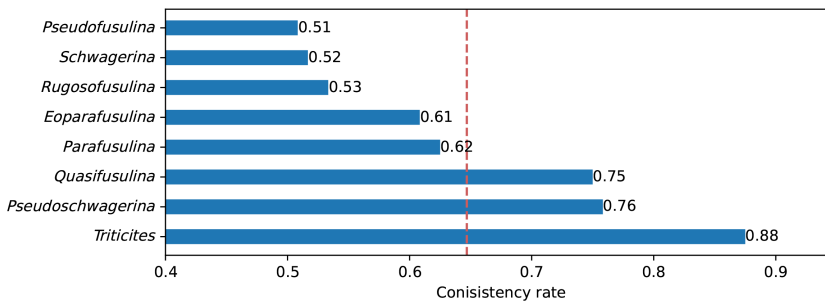


FIGURE 6 The mean consistency rate of each genus obtained in the consistency test of Table 4, calculated by pair comparison of dataset labels and results from the OGS model and two experts. The red dashed line indicates the total mean consistency rate across eight genera.

In the consistency test, two human experts are asked to identify 160 individual fusulinid images of 8 genera from Family Schwagerinidae, and their results are compared along with the labels (which can be seen as the collective ideas of many experts) and the inference output of OGS. The consistency rate between two identification results of n images is defined as n_{con}/n , where n_{con} is the number of images for which they gave consistent labels. Table 4 shows the

consistency matrix, where the consistency between two experts is the least at merely 53%, while OGS reaches the utmost consistency compared to all other inferences (85%, 68%, and 58%, with labels and two experts, respectively). This suggests that despite the many contradictions in specimen identifications among experts, the ensemble model still successfully captures the common features indicated by their collective ideas. Figure 6 looks into the problem from the perspective of different genera, and in line with the actual expert identification, *Pseudofusulina*, *Schwagerina* and *Rugosofusulina* hold the worst consistency of around 50%.

Consistency may be difficult to quantify in fossil identification problems, but if the model has undergone thorough training attempts, its optimal performance can provide some clues. In our case of fusulinids, a stable top-1 accuracy of 90-92% is gained in multiple training and testing processes of different base models (see Table 3), which points out that the labels support the generic delimitation of at least 90% of the involved individuals. However, the features involved are unclear, and may not be interpretable by a human. In the future study, the inconsistency can be better estimated and resolved by feature extraction using various methods including neural networks.

5 | CONCLUSIONS

Fossil identification is essential for evolutionary studies. Automatic identification models, especially recent advances based on deep learning, rely heavily on the quantity and quality of labeled images to train the models. However, the images are particularly limited for paleontologists due to the fossil preservation, conditioned sampling, and expensive and inconsistent label annotation by domain experts. To address these challenges, we proposed an innovative multiview ensemble framework that collects the multiple views of each fossil specimen image reflecting its different characteristics to train multiple base models and then makes the final decision via soft voting.

The proposed framework with original, gray, and skeleton views of fusulinids images for training can further improve from 0.81% top-1 accuracy (on the basis of 90.30% for RegNetY) to 2.32% top-1 accuracy (on the basis of 87.98% for ResNet-50) compared to the baseline using a single base model with original view. Furthermore, it obtained superior or similar performance compared to the method under the well-known bagging framework. Also compared to the baseline, the proposed framework can obtain more performance gains as the training ratio decreases, which demonstrated its superiority in the case of limited labeled data, e.g., obtaining about 6% top-1 accuracy gains (on the basis of about 69%) for ResNet-50 when train ratio decreases to 0.1. Moreover, the consistency test with two human experts showed the proposed method reached the greatest consistency with all identification results, indicating that it successfully integrated the ideas of multiple experts. We argue that the consistency of fossil identifications should be emphasized, and analysis and revision of labels should be considered before feeding data for model training. For future work, one interesting direction could be exploring other useful views that can capture different characteristics of images, and integrating these views into the proposed multiview ensemble framework. Besides, it is worth investigating adopting heterogeneous base models for the proposed framework, employing other techniques to combine the outputs of base models, and experimenting on more datasets of fossil images.

6 | ACKNOWLEDGEMENTS

This work was funded by the Natural Science Foundation of China under the Grant 42050101 and 42250104, the National Key R&D Program of China under the Grant 2018YFE0204201 and 2021YFB3600401, and the Fujian Provincial Natural Science Foundation under the Grant 2021J01586. This is also a contribution to the IUGS Deep-time Digital Earth Big Science Program.

7 | CONFLICT OF INTEREST

The authors declare no competing interests.

8 | AUTHORS' CONTRIBUTIONS

C.H. and X.L. conceived the ideas and designed the method; X.L. and C.H. wrote the code and conducted experiments; H.H. and Y.S. collected the data; X.L., H.H., C.H., and Y.S. analyzed the data; H.L. offered the computational resources; J. F., Y. S., and H. L. initiated the research idea; C.H., H.H., and X.L. wrote the manuscript; Y.S., H.L., S.X., and J.F. provided supervision and valuable comments, and revised the manuscript. All authors contributed critically to the drafts and gave final approval for publication.

References

- Behrensmeyer, A. K., Kidwell, S. M. and Gastaldo, R. A. (2000). Taphonomy and paleobiology. *Paleobiology*, 26 (S4), 103–147. doi:10.1017/S0094837300026907.
- Borowiec, M. L., Dikow, R. B., Frandsen, P. B., McKeeken, A., Valentini, G. and White, A. E. (2022). Deep learning as a tool for ecology and evolution. *Methods in Ecology and Evolution*, 13 (8), 1640–1660.
- BouDagher-Fadel, M. K. (2008). Chapter 2 the palaeozoic larger benthic foraminifera: the carboniferous and permian. In: BouDagher-Fadel, M. (Ed.) *Evolution and Geological Significance of Larger Benthic Foraminifera*. Vol. 21 of *Developments in Palaeontology and Stratigraphy*, pp. 39–118.
- Culverhouse, P. F., Macleod, N., Williams, R., Benfield, M. C., Lopes, R. M. and Picheral, M. (2014). An empirical assessment of the consistency of taxonomic identifications. *Marine Biology Research*, 10, 73–84. doi:10.1080/17451000.2013.810762.
- Dong, X., Yu, Z., Cao, W., Shi, Y. and Ma, Q. (2020). A survey on ensemble learning. *Frontiers of Computer Science*, 14 (2), 241–258.
- Fenton, I. S., Baranowski, U., Boscolo-Galazzo, F., Cheales, H., Fox, L., King, D. J., Larkin, C., Latas, M., Liebrand, D., Miller, C. G., Nilsson-Kerr, K., Piga, E., Pugh, H., Remmelzwaal, S., Roseby, Z. A., Smith, Y. M., Stukins, S., Taylor, B., Woodhouse, A., Worne, S., Pearson, P. N., Poole, C. R., Wade, B. S. and Purvis, A. (2018). Factors affecting consistency and accuracy in identifying modern macroperforate planktonic foraminifera. *Journal of Micropalaeontology*, 37, 431–443. doi:10.5194/jm-37-431-2018.
- Footo, M. and Raup, D. M. (1996). Fossil preservation and the stratigraphic ranges of taxa. *Paleobiology*, 22 (2), 121–140. doi:10.1017/S0094837300016134.
- He, K., Zhang, X., Ren, S. and Sun, J. (2016). Deep residual learning for image recognition. In: *Proceedings of the IEEE conference on computer vision and pattern recognition*. pp. 770–778.
- Holland, S. M. (2016). The non-uniformity of fossil preservation. *Philosophical Transactions of the Royal Society B: Biological Sciences*, 371 (1699), 20150130. doi:10.1098/rstb.2015.0130.
- Howard, A. G., Zhu, M., Chen, B., Kalenichenko, D., Wang, W., Weyand, T., Andreetto, M. and Adam, H. (2017). Mobilenets: Efficient convolutional neural networks for mobile vision applications. *arXiv preprint arXiv:1704.04861*.
- Hsiang, A. Y., Brombacher, A., Rillo, M. C., Mleneck-Vautravers, M. J., Conn, S., Lordsmith, S., Jentzen, A., Henehan, M. J., Metcalfe, B., Fenton, I. S., Wade, B. S., Fox, L., Meilland, J., Davis, C. V., Baranowski, U., Groeneveld, J., Edgar, K. M., Movellan, A., Aze, T., Dowsett, H. J., Miller, C. G., Rios, N. and Hull, P. M. (2019). Endless forams: >34,000 modern planktonic foraminiferal images for taxonomic training and automated species recognition using convolutional neural networks. *Paleoceanography and Paleoclimatology*, 34, 1157–1177. doi:10.1029/2019PA003612.

- Huang, H. and Shi, Y. (2022). Fusulinid images 2400 - nju. *DDE Repository*, doi:10.12297/dpr.dde.202211.5.
- Li, Z., Liu, F., Yang, W., Peng, S. and Zhou, J. (2021). A survey of convolutional neural networks: analysis, applications, and prospects. *IEEE transactions on neural networks and learning systems*,.
- Liu, X., Jiang, S., Wu, R., Shu, W., Hou, J., Sun, Y., Sun, J., Chu, D., Wu, Y. and Song, H. (2022). Automatic taxonomic identification based on the fossil image dataset (> 415,000 images) and deep convolutional neural networks. *Paleobiology*, 1–22. doi:10.1017/PAB.2022.14.
- MacLeod, N., Benfield, M. and Culverhouse, P. (2010). Time to automate identification. *Nature* 2010 467:7312, 467, 154–155. doi:10.1038/467154a.
- MacLeod, N., O'Neill, M. and Walsh, S. A. (2007). A comparison between morphometric and artificial neural network approaches to the automated species recognition problem in systematics. *Biodiversity Databases*, doi:10.1201/9781439832547-5.
- Marchant, R., Tetard, M., Pratiwi, A., Adebayo, M. and de Garidel-Thoron, T. (2020). Automated analysis of foraminifera fossil records by image classification using a convolutional neural network. *Journal of Micropalaeontology*, 39, 183–202. doi:10.5194/jm-39-183-2020.
- Martin, R. E. (1999). *Taphonomy: a process approach*. Vol. 4. : Cambridge University Press.
- Mitra, R., Marchitto, T. M., Ge, Q., Zhong, B., Kanakiya, B., Cook, M. S., Fehrenbacher, J. S., Ortiz, J. D., Tripathi, A. and Lobaton, E. (2019). Automated species-level identification of planktic foraminifera using convolutional neural networks, with comparison to human performance. *Marine Micropalaeontology*, 147, 16–24. doi:10.1016/J.MARMICRO.2019.01.005.
- Moore, R. C. (1964). *Treatise on Invertebrate Paleontology. Part C, Protista 2*. : Geological Society of America.
- Niu, Z.-B. and Xu, H.-H. (2022). Ai-based graptolite identification improves shale gas exploration. *bioRxiv*, doi:10.1101/2022.01.17.476477.
- Pawlowski, J., Holzmann, M., Berney, C., Fahrni, J., Gooday, A. J., Cedhagen, T., Habura, A. and Bowser, S. S. (2003). The evolution of early foraminifera. *Proceedings of the National Academy of Sciences of the United States of America*, 100, 11494–11498. doi:10.1073/PNAS.2035132100.
- Pires, R., Welch, K. F., Barrick, J. E., Marfurt, K. J., Burkhalter, R., Cassel, M. and Soreghan, G. S. (2020). Convolutional neural networks as an aid to biostratigraphy and micropaleontology: A test on late paleozoic microfossils. *PALAIOS*, 35, 391–402. doi:10.2110/palo.2019.102.
- Radosavovic, I., Kosaraju, R. P., Girshick, R., He, K. and Dollár, P. (2020). Designing network design spaces. In: *Proceedings of the IEEE/CVF conference on computer vision and pattern recognition*. pp. 10428–10436.
- Ross, C. A. and Ross, J. R. (1991). Paleozoic foraminifera. *BioSystems*, 25, 39–51. doi:10.1016/0303-2647(91)90011-9.
- Saha, P. K., Borgefors, G. and di Baja, G. S. (2016). A survey on skeletonization algorithms and their applications. *Pattern recognition letters*, 76, 3–12.
- Schopf, J. M. (1975). Modes of fossil preservation. *Review of Palaeobotany and Palynology*, 20 (1-2), 27–53. doi:10.1016/0034-6667(75)90005-6.
- Selvaraju, R. R., Das, A., Vedantam, R., Cogswell, M., Parikh, D. and Batra, D. (2016). Grad-cam: Visual explanations from deep networks via gradient-based localization. *International Journal of Computer Vision*, 128, 336–359. doi:10.48550/arXiv.1610.02391.
- Sheng, J., Zhang, L. and Wang, J. (1988). *Fusulinids*. : Science Press.

- Szegedy, C., Ioffe, S., Vanhoucke, V. and Alemi, A. A. (2017). Inception-v4, inception-resnet and the impact of residual connections on learning. In: *Thirty-first AAAI conference on artificial intelligence*.
- Szegedy, C., Liu, W., Jia, Y., Sermanet, P., Reed, S., Anguelov, D., Erhan, D., Vanhoucke, V. and Rabinovich, A. (2015). Going deeper with convolutions. In: *Proceedings of the IEEE conference on computer vision and pattern recognition*. pp. 1–9.
- Tan, M. and Le, Q. (2019). Efficientnet: Rethinking model scaling for convolutional neural networks. In: *International conference on machine learning*. PMLR, pp. 6105–6114.
- Vachard, D., Pille, L. and Gaillot, J. (2010). Palaeozoic foraminifera: Systematics, palaeoecology and responses to global changes. *Revue de Micropaléontologie*, 53, 209–254. doi:10.1016/J.REVMIC.2010.10.001.
- Wäldchen, J. and Mäder, P. (2018). Machine learning for image based species identification. *Methods in Ecology and Evolution*, 9 (11), 2216–2225.
- Wilf, P., Wing, S. L., Meyer, H. W., Rose, J. A., Saha, R., Serre, T., Cúneo, N. R., Donovan, M. P., Erwin, D. M., Gandolfo, M. A., González-Akre, E., Herrera, F., Hu, S., Iglesias, A., Johnson, K. R., Karim, T. S. and Zou, X. (2021). An image dataset of cleared, x-rayed, and fossil leaves vetted to plant family for human and machine learning. *PhytoKeys*, 187, 93–128. doi:10.3897/PHYTOKEYS.187.72350.
- Zhang, T. Y. and Suen, C. Y. (1984). A fast parallel algorithm for thinning digital patterns. *Communications of the ACM*, 27 (3), 236–239.
- Zhou, B., Khosla, A., Lapedriza, À., Oliva, A. and Torralba, A. (2015). Learning deep features for discriminative localization. *2016 IEEE Conference on Computer Vision and Pattern Recognition (CVPR)*, 2921–2929.
- Zhou, Z.-H. (2021). Ensemble learning. In: *Machine learning*, pp. 181–210.
- Zoph, B. and Le, Q. V. (2016). Neural architecture search with reinforcement learning. *arXiv preprint arXiv:1611.01578*.